

Inkjet printing of epitaxially connected nanocrystal superlattices

Daniel M. Balazs[†], N. Deniz Erkan, Michelle Quien, and Tobias Hanrath ()

School of Chemical and Biomolecular Engineering, Cornell University, Ithaca, NY, USA
† Present address: Institute of Science and Technology Austria, Am Campus 1, Klosterneuburg 3400, Austria

© Tsinghua University Press and Springer-Verlag GmbH Germany, part of Springer Nature 2021

Received: 22 September 2021 / Revised: 4 November 2021 / Accepted: 19 November 2021

ABSTRACT

Access to a blossoming library of colloidal nanomaterials provides building blocks for complex assembled materials. The journey to bring these prospects to fruition stands to benefit from the application of advanced processing methods. Epitaxially connected nanocrystal (or quantum dot) superlattices present a captivating model system for mesocrystals with intriguing emergent properties. The conventional processing approach to creating these materials involves assembling and attaching the constituent nanocrystals at the interface between two immiscible fluids. Processing small liquid volumes of the colloidal nanocrystal solution involves several complexities arising from the concurrent spreading, evaporation, assembly, and attachment. The ability of inkjet printers to deliver small (typically picoliter) liquid volumes with precise positioning is attractive to advance fundamental insights into the processing science, and thereby potentially enable new routes to incorporate the epitaxially connected superlattices into technology platforms. In this study, we identified the processing window of opportunity, including nanocrystal ink formulation and printing approach to enable delivery of colloidal nanocrystals from an inkjet nozzle onto the surface of a sessile droplet of the immiscible subphase. We demonstrate how inkjet printing can be scaled-down to enable the fabrication of epitaxially connected superlattices on patterned sub-millimeter droplets. We anticipate that insights from this work will spur on future advances to enable more mechanistic insights into the assembly processes and new avenues to create high-fidelity superlattices.

KEYWORDS

interfacial assembly, colloidal nanocrystal, superlattice, inkjet printing

Directing the assembly of colloidal nanocrystal (NC) building blocks into ordered superstructures is of broad scientific and technological interest. Interactions between the constituent nanocrystals in the superlattice (SL) can give rise to emergent properties, which can be programmed provided that the SL structure can be adequately controlled. The technological implications of this emerging class of metamaterials [1] are profound with potential applications in diverse technologies ranging from electronics [2, 3], photovoltaics [4], thermoelectrics [5, 6], and catalysis [7-9]. Bringing the heralded prospects of NC assemblies to fruition is contingent on better understanding of and control over the formation mechanism and the emerging structure-property relationships; both of these tasks rely critically on access to high-fidelity SLs. Many of the current practical challenges to assembling colloidal NCs into highly ordered SLs derive from the complexity of the interactions between NCs and the interplay between different transport phenomena that occur during the assembly. The current stage of knowledge concerning the underlying molecular interactions has been discussed in several excellent reviews [10, 11].

The interface between two immiscible fluids provides a versatile and effective experimental platform to direct the self-assembly of high-fidelity NC assemblies. Earlier studies [12, 13] of interfacial self-assembly have illustrated two key advantages: (i) Uniform NC layers can be readily formed over large areas (cm²), (ii) The assembled structures are sufficiently robust to enable their transfer to solid supports (e.g., substrates with contact electrodes). More

recently, the ability to expose the NC assembly to chemical treatments from the liquid side of the interface has been established as another key advantage of this approach. Several groups have demonstrated that chemical treatments of pre-assembled NC assemblies at fluid interfaces can transform the assembly of ligand-passivated NCs into an epitaxially connected superlattices (epi-SLs) [14-20]. Epi-SLs have garnered significant scientific interests as a programmable material system whose properties can be tailored by the balance of quantum-confinement of NC building blocks and quantum-coupling between them. The observation of micrometer-sized grains of epi-SLs is remarkable considering that their formation involves the irreversible attachment of on the order of 104-105 NCs. Charge transport in epi-SLs has been examined by several groups [17, 21-23] and led to the emerging consensus that the structural fidelity of currently available superlattices is insufficient to realize the predicted emergent properties arising from long range charge delocalization [24, 25]. Recent detailed structural studies have pointed to the role of microscopic misalignments in the initial assembly as a key culprit of disorder and defects in epi-SLs [26, 27]. As with classical crystallization processes, it is important to recognize that the defect density in epi-SLs is directly related to assembly and processing conditions. In specific, the initial interfacial NC assembly is sensitive to a complex choreography of several physicochemical processes including spreading of the solution, evaporation of the solvent, and recession of the vapor-liquid interface as was revealed in a recent in-situ grazing-incidence small-angle X-ray scattering (GISAXS) study by our group [28].

Collectively, recent interfacial assembly and attachment studies point towards the need for more advanced processing methods to provide refined control over the delivery of the NC solution to the fluid interface. The volume of the deposited solution is a key consideration in the process of creating a liquid thin film from which NCs assemble on the surface of the sessile liquid subphase and attach to form epi-SLs. Considering a typical NC colloidal concentration in the range of $\sim 2-300 \text{ mg}\cdot\text{ml}^{-1}$, the formation of a monolayer NC film requires deposition of an ink film thickness of a least 100 nm. In the case of microliter droplets deposited from a conventional micropipettor, this film thickness requires spreading across an interface area of ~ 10² cm² [28]. Translating processing insights from earlier studies with cm2 scale surfaces to smaller interfaces in which dynamic processes can be better controlled therefore requires the ability to deposit smaller solution volumes. In this context, the ability of inkjet printers to deliver small (typically picoliter) liquid volumes with precise positioning is very attractive for both scientific and technological reasons. For example, Minemawari et al. [29], successfully demonstrated inkjet printing of single crystals of organic semiconductors on the surface of a micrometer-sized antisolvent droplet. Beyond providing an experimental testbed to refine our mechanistic understanding of the assembly and attachment, inkjet printing of NC assemblies at fluid interfaces also has notable technological implications as this fabrication strategy could enable creation of epi-SLs in more complex geometries required for device integration. Inspired by these prospects, we set out to translate this approach to enable the delivery of colloidal NCs on top of an immiscible fluid interface. In this work, we sought to build on these insights to identify a window of opportunities (including ink formulation and printing approach) to enable delivery of colloidal NCs onto the surface of a sessile droplet. We anticipated that insights from this work will spur on future advances to enable more mechanistic insights into the assembly processes and new avenues to create high-fidelity superlattices.

Key aspects of the inkjet printing of NC solutions on the surface of an immiscible sessile droplet are schematically summarized in Fig. 1. In this approach, picoliter-scale droplets are accelerated to relatively high velocity (m·s⁻¹) in a drop-on-demand system that is activated by piezoelectric or thermal elements [30]. Figure 1 illustrates the sequence of processing stages including the initial formation of a droplet of the NC solution (i.e., jetting), the subsequent "landing" of the droplet on the fluid interface, and ultimate transformation of the droplet into an epi-SL as the solvent spreads and evaporates. Below, we examined the coupled physicochemical and fluid mechanical constraints of these

We started by summarizing critical considerations for ink formulation, and how they can be realized for the colloidal NC inks for interfacial assembly. The formation of a droplet by the periodic motion of a piezoelectric nozzle (i.e., jetting) is a fluid transport process which is sensitive to the rheological properties of the ink (mainly viscosity and surface tension) [31]. Optimized inks typically consist of three types of ingredients: solute, solvent, and additives that together enable efficient processing. Conditions for depositing inks onto solid substrates have been established and applied in many industries [31-33]. More specifically, inkjet printing of NC solutions has recently been successfully demonstrated for a range of NC-based devices [34–37]. Moreover, success with two-component crystallization of organic molecules and polymer colloids on the sub-mm scale suggests the technique can be applied to more complex systems as well [29, 38, 39]. We reviewed the ingredients one-by-one in context of both jetting and interfacial assembly of epi-SLs.

Solute: The formation of epi-SLs requires building blocks with (i) good stability in solution [28], (ii) dynamically bound ligand shell that allows gradual ligand removal [18], and (iii) some degree of ligand shell anisotropy, the presence of facets with lower surface energy and corresponding lower ligand coverage that can form the epitaxial necks [14, 19, 40]. Lead sulfide and selenide nanocrystals capped with oleic acid fulfil these requirements, and serve as great model systems. The stability of the colloidal NC solution is governed, in large part, by the nature of the interactions between the solvent and the ligands bound to the NC surface; on the solute side, it is defined by the ligand density. The post-synthesis processing of the colloidal NC solutions typically involves purification via precipitation induced by addition of a non-solvent. The choice of polar non-solvent can impact the integrity of the NC ligand shell; whereas aprotic and weak nucleophile solvents (nitriles and ethers) have relatively little impact on the ligand shell, protic or strongly coordinating ones (alcohols and amines) typically lead to significant ligand loss [18, 41–43].

Solvent: As the solvent is the carrier for the NCs, good solubility and solution stability are required. Stable colloidal solutions of our model PbSe NCs can be formed in a range of apolar solvents, better in alkanes than in arenes [28]. Moreover, for the specific case of interfacial assembly, there are requirements associated with the subphase. The formation of a stable interface on which the NCs can spread and assemble implies immiscibility between the subphase and all ingredients of the ink. Homogeneous films require complete wetting; the energetics of wetting are parametrized by the spreading coefficient $S = \gamma_{AC} - (\gamma_{AB} + \gamma_{BC}) > 0$, where A is air, B is top, and C is bottom liquid. This scenario is typically achieved when the surface tension of the subphase γ_{AC} is rather high (typically using polar and high boiling point subphases). The immiscibility of the colloidal NC solutions and the subphase requires chemical dissimilarity, which can also cause non-wetting in the case of high interfacial energy between the top and bottom fluid (γ_{BC} , e.g., benzene and water). Collectively, the dual demands for desired spreading and immiscibility point to a delicate balance of the fluid properties of the NC-containing droplet and the sessile drop (also referred to as the subphase). Mono- and oligoethylene glycols have been established as suitable subphases for NCs

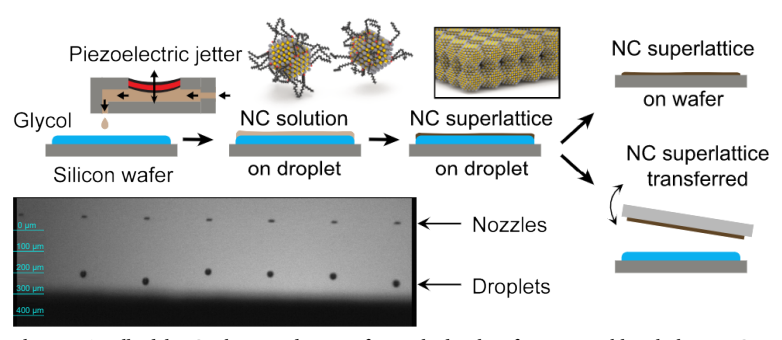


Figure 1 Sketch of the experimental setup. A colloidal NC ink is jetted on to of a sessile droplet of an immiscible subphase. NCs in the thin liquid film then assemble and attach to form an epitaxially connected superlattices (epi-SLs) which can subsequently be transferred to a solid substrate.

dissolved in hydrocarbons [13, 14, 17]. These subphases facilitate the spreading of alkanes and arenes (especially hexane, decane, and toluene), which are typically used in these experiments. This immiscibility requirement excludes the use of ethers, ketones, and chlorinated solvents.

Additives: For the specific application in inkjet printers, optimized ink formulations typically contain additives to solvent and solute to aid in the jetting of the ink. Whereas this approach works well for inks deposited and dried onto solid targets, it is not viable for jetting onto liquid droplets with the intent of forming thin films that ultimately transform into epi-SLs. We did not examine viscosity modifying additives in our NC ink formulation since we expect that the presence of surface active (e.g., isopropanol) or high viscosity (e.g., glycerol) additives would interfere with film formation, spreading, NC assembly as well as the ultimate attachment of epi-SLs.

Droplet formation: The processing window of opportunity for stable inkjet printing is constrained by several factors. The inertial energy of the droplet has to be sufficiently high to be ejected from the nozzle as a droplet, but not too high to splash upon impact with the target. Similarly, the rheology of the ink must be tailored to attain a viscosity that is low enough to enable jetting, but not too low to avoid complications of the droplet breaking up into smaller satellites [31]. This latter stability range is typically described as the dimensionless Ohnesorge number (Oh) being between 1/4 and 1/14, although the exact range depends on the experimental conditions [30, 31, 44, 45]. The Ohnesorge number hence provides a convenient metric to guide the identification of ink properties (viscosity, density, and surface tension) to form jettable droplets. These constraints can be expressed in terms of the more intuitive Reynolds number ($Re = \rho v d/\mu$) and Weber number $(\text{We} = \rho v^2 d/\gamma)$ as We < 1/16 Re², We > 1/200 Re² (for droplet stability), and We > 4 (for ejection), where ν , d, ρ , μ , and γ represent the droplet velocity and diameter, solvent density, viscosity, and surface tension, respectively. In conventional inks, a wide range of solvents can be made jettable by using additives. In our case, the choice of solvent is the only free parameter.

The fluid mechanical constraints are conveniently illustrated as a processing window of opportunity in the Re–We space (Fig. 2) as discussed by Derby [31] or in terms of the capillary number in Ca–We space as discussed by Nallan [30] for the specific case of nanoparticle inks. To identify suitable ink solvents, we calculated the Re and We values for common apolar solvents that are expected to meet the chemical and interfacial compatibility constraints; the data are shown in Fig. 2(a). Based on the specifications of the material printer, our experiments were performed with $\sim 30~\mu m$ diameter droplets accelerated to a velocity of $\sim 3~m \cdot s^{-1}$. To a first approximation, we assumed that the

rheology of the ink is dominated by the properties of the solvent (neglecting the effect of the colloidal solute). This preliminary screening analysis suggests that most common solvents, including hexane and toluene, are not sufficiently viscous to enable stable jetting. Based on this parameter analysis, we shifted our focus to long-chain hydrocarbons such as n-dodecane, n-tetradecane, 1-octadecene, and squalene as sufficiently viscous solvents for jettable inks.

We refined our analysis of the physical properties of the colloidal ink by considering the effect of the colloidal NCs on the rheology of the solution [46]. The solution density can be approximated as the volume-weighted arithmetic mean of the values for the pure solvent and the NC material (assuming 6 nm cores). The surface tension is not expected to change given the strong similarity of the ligands and the solvent [47]. The dynamic viscosity can be estimated as $\mu(\varphi) = \mu(0) \cdot (1 - \varphi/\varphi_{\text{max}})^{-n}$, where φ is the volume fraction including the ligand shell (we used a total diameter of ter of ~ 10 nm), μ (0) is the solvent viscosity, $\varphi_{\rm max}$ is the value at which the viscosity diverges to infinity, and $n = 5/2 \cdot \varphi_{\text{max}}$ for spheres [48]. We recently reported that oleate-capped NCs behave as hard spheres in good solvents at these concentrations, and that the observable φ_{max} is ~ 0.55 (belonging to a concentration of ~ 2 mM, ~ 1, 100 g·L⁻¹) [28]. Accounting for the impact of the colloidal NC on the viscosity and density of the ink suggests that Re is reduced by about 15% whereas We is increased by about 30%. In the language of the Re-We plot in Fig. 2, this means that the addition of the NC to the solvents that are not jettable in pure form can transition into the "printable window". We noted that the boundaries of the processing window in Re-We space should be considered as a blurry regime rather than a sharp cut-off.

Having analyzed the conditions required for jetting of the colloidal NC ink, we now turn our attention to the subsequent steps of droplet impingement, spreading, and evaporation illustrated in Fig. 1. As with all things that fly, the jetted droplet will subsequently land on a surface. To avoid splashing of the sessile droplet, the ratio of inertial to viscous forces is constrained below a critical threshold which is numerically reflected in the modified Weber number, We' = $\rho v^2 d^3/y_s h_s^2$ (where the "s" subscript indicates subphase property) having a value < 1 [38]. To visualize it with the other constraints, the We' criterion can be reduced to a limit in regular Weber number set as We $< \gamma_s h_s^2/\gamma_s d^2$; this relationship illustrates the crucial dependence on the sessile droplet thickness. The constraint of the minimum thickness of the sessile droplet is shown in Fig. 2(b) for the n-dodecane ethylene-glycol pair for the observed inkjet droplet characteristics. The basic theoretical model suggests that the minimum sessile droplet thickness for the studied system is around ~ 60 µm.

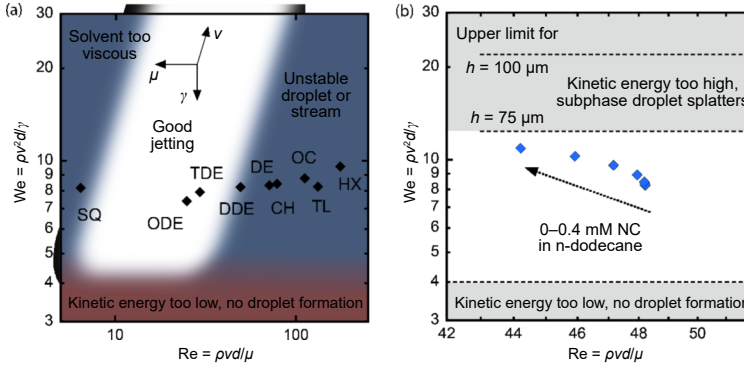


Figure 2 (a) Fluid mechanical constraints of the jetting process and example values calculated for a set of possible solvents (HX: n-hexane, TL: toluene, OC: octane, CH: cyclohexane, DE: n-decane, DDE: n-dodecane, TDE: n-tetradecane, ODE: 1-octadecene, and SQ: squalene), the inset arrows show the effect of the material properties on the marker positions. (b) Upper limits for the Weber number as function of sessile droplet thickness *h*, calculated for ethylene glycol (subphase) and PbSe NCs in n-dodecane.

Following the impingement on the fluid surface, the droplet should spread and evaporate, which introduces additional criteria with regards to ink formulation and processing conditions. As discussed above, the spreading behavior across a fluid interface is governed by the surface tension; in the case of alkanes, the surface tension increases with the chain length, which bars longer chain molecules from spreading on polar subphases. For example, based on predictions of the simple spreading coefficient model, alkanes up to n-heptane are expected to spread on water at room temperature, whereas n-octane and longer do not [49, 50]. We experimentally confirmed that the robustness of the spreading process on ethylene glycol (EG) decreases with the increasing chain length; however, we found that n-decane and n-dodecane can still spread easily in most experiments, whereas n-tetradecane did not. The alkanes that spread on EG show enough surface pressure to cover the droplet with a precursor film within a fraction of a second, and fully spread into a rather homogeneous film within seconds [28].

Lastly, the volatility of the solvent presents an important design consideration to ensure solvent evaporation in a practical timeframe (~ 1–100 min). This time range reflects the fact that the solvent volatility should be: (i) low enough to avoid solvent loss during jetting and enable spreading of the colloidal solution, yet (ii) high enough to evaporate once the solution has spread and NCs have assembled. C₁₀-C₁₄ alkanes are generally suitable in context of the volatility constraints. Extended evaporation time with low volatility solvents can be problematic as NCs within the assembly may start to neck under uncontrolled conditions due to the dynamic nature of ligands bound to the NC surface. Although higher viscosity solvents such as 1-octadecene and squalene satisfy the jetting criterion, they fail the volatility requirement since they would require acceleration via vacuum or heating, and both processes would likely interfere with the assembly and attachment process [14]. We have previously shown that high-quality films of NCs can be formed using n-decane [28] or n-dodecane [26] when the volume is adjusted to the through size to evaporate in 30-60 s. Our previous study of interfacial NC assembly showed that the sub-processes of solvent spreading and evaporation are kinetically coupled and this interplay has an important impact on the structure of the formed assemblies [28]. Based on the coupled constraints of jetting, spreading and evaporation discussed above, this parameter analysis pointed to n-dodecane as the most promising solvent for inkjet printing-based interfacial assembly.

We performed a series of inkjet printing experiments to confirm n-dodecane as a suitable solvent. A Fujifilm Dimatix DMP-2800 Material Printer and nominally 10 pL droplet volume cartridges were used. We fine-tuned the voltage pattern of the piezoelectric nozzle to optimize droplet formation as illustrated by the reliable jetting for both pure n-dodecane and a concentrated NC solution (Fig. 1). The video recordings reveal an average droplet diameter (~ 29 µm), volume (~ 13 pL), and velocity (~ 3 m·s⁻¹). For our experiments, we used ~ 6.4 nm PbSe NCs capped with oleic acid synthesized following established protocols [28]. We printed a number of ink droplets onto EG subphase confined in ~ 3 mm radius hemispherical polytetrafluoroethylene (PTFE) wells ($\sim 60~\mu L$). The concentration (close to the solubility limit of the NCs in n-dodecane) was set so that 80-200 nm thick liquid films would result in 1-3 monolayer (ML) thick superlattices. In these conditions, we estimated the drying time to be 30-120 s [26]. The required volume for these wells was about 300 droplets per SL monolayer. Injected at 5 kHz, the injection time was a total of 60 ms per ML, the same order of magnitude as the precursor film formation. The spreading (estimated to occur within a few seconds) and drying (30-120 s) took place on an undisturbed sessile droplet.

The true appeal of the epi-SLs lies in our ability to convert them to single-crystalline and confined-but-connected arrays of quantum objects through controlled epitaxial necking. We triggered the epitaxial attachment of NC within the SL by injecting 1 μL of ethylenediamine (EDA) into the wells [17, 20]. The films were transferred to transmission electron microscopy (TEM) grids via stamping; the obtained images of a series of assemblies with and without chemically triggered NC attachment are shown in Fig. 3. We calculated the nominal film thicknesses given in units of NC layers based on the number of jetted droplets (ranging from 200 to 1, 000), the solution concentration (0.26 mM), the mean particle area in the observed lattice (6.5-8.2 nm spacing in various geometries), and the well area (~ 30 mm²). Visually good thickness scaling was observed in both the initial and connected superlattices. This aspect is crucial for reliable printing of small area films and underscores the viability of using inkjet printing to create NC assemblies and epi-SLs at fluid interfaces.

Structural analysis of the resulting NC assemblies showed that the NCs form disordered hexagonal arrays in sub-monolayer films. Thicker films form body-centered cubic (BCC) superlattices with a <110>_{SL} orientation normal to the fluid interface and micrometer-scale grains (see fast Fourier-transforms (FFT) patterns in Fig. 3). Selected-area electron diffraction (SAED) patterns inform the atomic orientation of NC building blocks within the assembly. The NCs in both 0.75 and 1.5 ML films show a dominant <100>AL orientation. The sub-monolayer film is more disordered with a considerable fraction of the NCs tilted off-axis since a faint {311}_{AL} or {222}_{AL} diffraction ring is present. The inplane order is nonexistent in the case of 0.75 ML sample, while the 1.5 ML film show a preferred in-plane orientation of the NCs, though with a significant azimuthal broadening indicating only a weak preference. By contrast, the thicker 3.5 ML sample show welldefined diffraction pattern confirming a preferred <110>AL orientation of the NCs. This transition is related to the interfacial potential landscape. Monolayer films on EG subphase have a strong preference for <100>AL orientation in a hexatic or square lattice [14, 26, 51], while bulk samples prefer a <110>AL orientation and a <110>_{SL}-oriented BCC lattice [19, 28, 52]. It is important to mention that the orientation is not precise <110>AL, but rather something derived from it through a minor tilt [19, 52]. The transition occurs at 2-3 monolayers (MLs), either by forcing the first layer to take an energetically less favored structure or by gradual straining into the new structure, similarly to the Frank-van der Merwe growth mechanism in epitaxial systems. All these findings are in agreement with previous observations on samples prepared manually, highlighting the applicability of inkjet printing for the formation of NC superlattices.

We examined the structure of NC assemblies that were converted to epi-SLs upon chemical treatment with EDA. The EDA treatment reduces the NC ligand coverage [18], changes the interaction potential between proximate NCs and leads to a change in superlattice structure (from body-centered cubic to simple cubic) and ultimately epitaxial attachment of osculant particles [53, 54]. The TEM images and accompanying electron diffraction in Fig. 3 show that the EDA treated samples transformed towards <100>_{SL}-oriented simple cubic structures. The 0.75 and 1.5 ML samples exhibit a two-dimensional (2D) rhombic lattice whereas the 3.5 ML film can be described as a rhombohedral epi-SL. At the same time, the orientational disorder of constituent NCs in the assembly narrows (indicated by the sharper features). These findings are in line with previous observations where the ligand desorption forces the particles to turn face-to-face and induces epitaxial directed attachment of proximate NCs [14, 18, 19, 26]; nevertheless, there are several important differences. First, the degree of order in these samples is

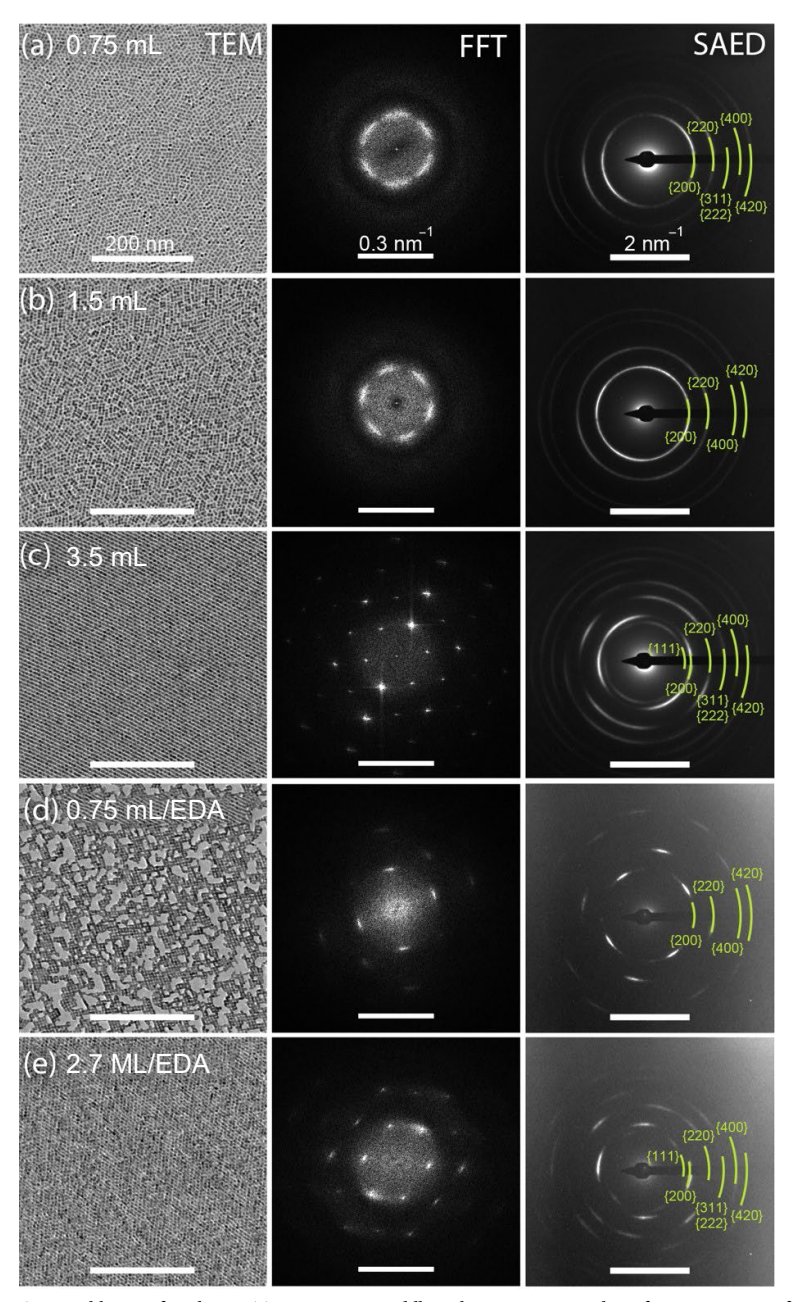


Figure 3 Structure analysis of NC assemblies. Left column: TEM images, middle column: corresponding fast Fourier-transforms (FFT), and right column: representative selected area electron diffraction (SAED) patterns of samples prepared by jetting various number of NC ink droplets onto an EG surface, before (a)–(c) and after (d) and (e) chemically triggered attachment.

substantially lower than in samples prepared on large troughs in a nitrogen-filled glovebox. Second, many cases of dimer formation, i.e., premature necking of proximate NCs are observed [26–28]. Such trends have been observed in similar experiments performed by conventional interfacial assembly performed in a glovebox with high oxygen content (in the range of 1–20 ppm $\rm O_2$), suggesting that that the initial disorder is related to the processing being performed in air [55]. Second, the transition to the simple cubic superlattice is not complete, lattice angles of 75°–80° instead of > 85° are found in both thin and thick films. Lastly, the NCs are not oriented <100> $\rm AL$ normal to the fluid interface in the multilayer assemblies. Collectively, these discrepancies suggest that the effect of air includes a hindrance to perfect transformation, likely through premature destabilization of the ligand coverage of the $\rm \{100\}_{AL}$ facets [56].

Since inkjet printing enables new opportunities to form NC assemblies with smaller ink volumes and interface areas, we examined the prospects of downscaling the fabrication process.

Stable sessile droplets of 1 mm × 2 mm or smaller were formed on a solid surface by two methods. At first, the droplets were confined using wetting contrast, hydrophilic areas in a hydrophobic surrounding created by area-selective ozonolysis of a hexamethyldisilazane (HMDS)-coated Si surface [29]. EG droplets were successfully created via this method, but the NC solution wetting the surrounding area made the formation of high-quality films on the droplets difficult. A modified approach of inverting the pattern and creating a perfluorooctyltrichlorosilane (FOTS) coating rendering most of the surface non-wetting was found to be more suitable. The contrast in chemical functionality was sufficiently strong to allow droplet formation simply by immersing the wafer into EG. However, the strongly non-wetting fluorinated surface showed limited to zero edge-pinning; the droplet shape tended to be independent of that of the wettable pattern, limiting the control over deposition shape and surface area. As an alternative approach, we created confinement for sessile droplets by etching 100 µm deep wells into a Si wafer. The wetting contrast

was enhanced by ozonolysis, rendering the surface hydrophilic. This way we were able to form stable EG droplets and created NC superlattices thereon.

Figure 4 shows the images collected from a sample prepared on a geometrically contained droplet. The low magnification TEM image shows the shape of the droplet on the grid, implying that NC film spreads around the whole droplet, and NC superlattices can be reliably created on mm scale. Higher magnification images confirm the local thickness homogeneity and ordered superlattice

similar to those obtained using large-scale experiments [28]. The dark rim-like feature and the numerous cracks inside the film suggest that there is a significant edge effect. Specifically, the spreading is hindered near the edges causing accumulation, and the shrinkage following the drying of the film occurs not on a free-floating, rather an edge-pinned film. Further fine-tuning the four-phase (air, ink, subphase, and substrate) contact line behavior in alignment with the required work on wetting contrast is required to resolve this challenge.

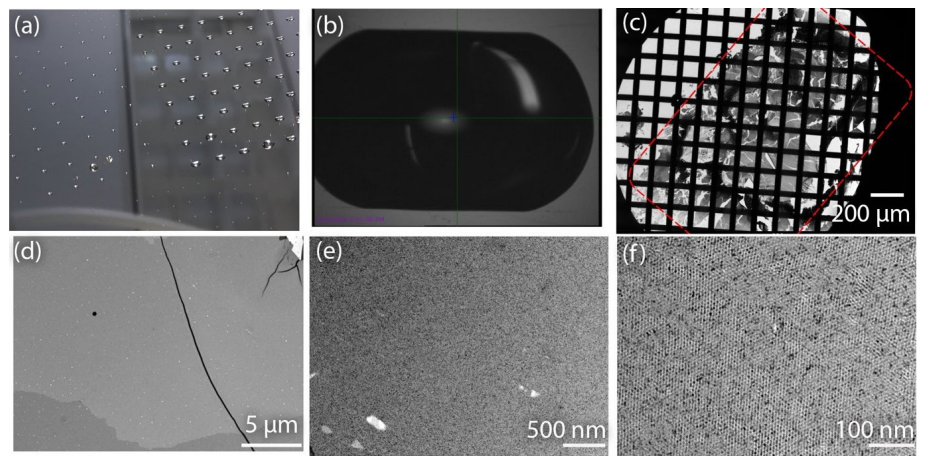


Figure 4 Multi-scale analysis of NC printed on patterned droplet. (a) Optical image of droplets formed by spreading ethylene glycol on a patterned-fluorinated substrate. (b) Optical micrograph image of such a droplet. (c) TEM image of a ~ 3 monolayer thick NC film prepared on a 1-by-1.5 mm droplet by inkjet printing; the shape of the droplet is marked showing complete spreading and coverage. (d)-(f) The local homogeneity and superlattice structure are similar to those of samples prepared on larger scale.

While we showed that the approach works on a $\sim 1 \text{ mm}^2$ scale, the process can in principle be scaled further down. Working with inks of this concentration, a single droplet can create a monolayer of 0.08 mm² or 200 μ m \times 400 μ m, or a 100 nm thick assembly of 70 μ m \times 70 μ m. This samples size is similar to the minimum thickness of a stable sessile droplet (Fig. 2), highlighting that a 3D confinement of the sessile droplet used in the last section may actually be more suitable for scalability. On the other hand, this length-scale is similar to the pixel size in pixel array detectors used for electron and X-ray detection, allowing for the development of new fabrication concepts that leverage access to well-defined single crystal epi-SLs.

Whereas the inkjet printing process enables fabrication of NC assemblies and epi-SLs on smaller interface areas, we also noted several limitations of the described film formation method set by the configuration of our current setup. The most important aspect is the ambient environment of the printer in a regular laboratory without secondary containment to control oxygen and moisture content in the atmosphere. The commercially available casing that provides safety for the tool and the operator is not designed to host delicate chemical experiments. First, the EG evaporation rate depends on the ventilation and the temperature, which can affect the time available for the superlattice formation and introduce an uncertainty in the droplet size. Integrating the sessile droplet creation into the jetting equipment (as reported by Minemawari et al.)[29] and working in an atmosphere saturated with EG will likely lead to more controllable deposition. Second, the spreading of n-dodecane on EG can be hindered by contamination that affects the surface tension, which we observed frequently. A closed system with only the ink and the subphase present will enable a more robust process. Third, the effect of ambient air on the NC ink needs to be mitigated. While we made the utmost effort in maintaining the ink quality, filling the cartridge in an inert glovebox, and exposing the ink to air only for the actual printing process, we observed the sign or air-related excess reactivity in each sample. This suggests that the subphase needs to be handled in inert conditions as well. Fourth, a method to trigger the ligand desorption and epitaxial necking needs to be developed. At such scales, precise injection into the subphase is becoming an issue; a gas-phase chemical trigger could be suitable. Alternatively, triggering reactants already present in the sessile droplet by illumination could simplify the process [57]. In conclusion, an inkjet printer placed in a controlled, inert environment will enable robust processing of NC superlattices at the sub-millimeter scale. The above-described design principles will allow researchers to create a system that produces epitaxially connected NC superlattices in a reliable manner. The process can then be integrated into fabrication lines, or used as a screening method for crystallization or reaction kinetics, testing subphases, triggers, building blocks, or any other parameter of interest.

Acknowledgments

This project was supported by the US Department of Energy through award (No. DE-SC0018026). The work was performed in part at the Cornell NanoScale Facility, a member of the National Nanotechnology Coordinated Infrastructure (NNCI), which is supported by the National Science Foundation (No. NNCI-1542081) and in part at the Cornell Center for Materials Research with funding from the NSF MRSEC program (No. DMR-1719875). The authors thank Beth Rhodes for the technical assistance with inkjet printing, and E. Peretz and Q. Wen for the early exploratory experiments.

Electronic Supplementary Material: Supplementary material (literature overview of jetting limits) is available in the online version of this article at https://doi.org/10.1007/s12274-021-4022-7.

References

[1] Nie, Z. H.; Petukhova, A.; Kumacheva, E. Properties and emerging



- applications of self-assembled structures made from inorganic nanoparticles. *Nat. Nanotechnol.* **2010**, *5*, 15–25.
- [2] Kagan, C. R.; Lifshitz, E.; Sargent, E. H.; Talapin, D. V. Building devices from colloidal quantum dots. *Science* 2016, 353, aac5523.
- [3] Talapin, D. V.; Lee, J. S.; Kovalenko, M. V.; Shevchenko, E. V. Prospects of colloidal nanocrystals for electronic and optoelectronic applications. *Chem. Rev.* 2010, 110, 389–458.
- [4] Nozik, A. J.; Beard, M. C.; Luther, J. M.; Law, M.; Ellingson, R. J.; Johnson, J. C. Semiconductor quantum dots and quantum dot arrays and applications of multiple exciton generation to third-generation photovoltaic solar cells. *Chem. Rev.* 2010, 110, 6873–6890.
- [5] Vineis, C. J.; Shakouri, A.; Majumdar, A.; Kanatzidis, M. G. Nanostructured thermoelectrics: Big efficiency gains from small features. Adv. Mater. 2010, 22, 3970–3980.
- [6] Urban, J. J. Prospects for thermoelectricity in quantum dot hybrid arrays. Nat. Nanotechnol. 2015, 10, 997–1001.
- [7] Zhou, Z. Y.; Tian, N.; Li, J. T.; Broadwell, I.; Sun, S. G. Nanomaterials of high surface energy with exceptional properties in catalysis and energy storage. *Chem. Soc. Rev.* 2011, 40, 4167–4185.
- [8] Crabtree, G. W.; Sarrao, J. L. Opportunities for mesoscale science. MRS Bull. 2012, 37, 1079–1088.
- [9] Henry, C. R. 2D-arrays of nanoparticles as model catalysts. *Catal. Lett.* 2015, 145, 731–749.
- [10] Min, Y.; Akbulut, M.; Kristiansen, K.; Golan, Y.; Israelachvili, J. The role of interparticle and external forces in nanoparticle assembly. *Nat. Mater.* 2008, 7, 527–538.
- [11] Bishop, K. J. M.; Wilmer, C. E.; Soh, S.; Grzybowski, B. A. Nanoscale forces and their uses in self-assembly. *Small* 2009, 5, 1600–1630.
- [12] Lambert, K.; Čapek, R. K.; Bodnarchuk, M. I.; Kovalenko, M. V.; Van Thourhout, D.; Heiss, W.; Hens, Z. Langmuir-schaefer deposition of quantum dot multilayers. *Langmuir* 2010, 26, 7732–7736.
- [13] Dong, A. G.; Chen, J.; Vora, P. M.; Kikkawa, J. M.; Murray, C. B. Binary nanocrystal superlattice membranes self-assembled at the liquid-air interface. *Nature* 2010, 466, 474–477.
- [14] Evers, W. H.; Goris, B.; Bals, S.; Casavola, M.; De Graaf, J.; Van Roij, R.; Dijkstra, M.; Vanmaekelbergh, D. Low-dimensional semiconductor superlattices formed by geometric control over nanocrystal attachment. *Nano Lett.* 2013, 13, 2317–2323.
- [15] Boneschanscher, M. P.; Evers, W. H.; Geuchies, J. J.; Altantzis, T.; Goris, B.; Rabouw, F. T.; Van Rossum, S. A. P.; Van Der Zant, H. S. J.; Siebbeles, L. D. A.; Van Tendeloo, G. et al. Long-range orientation and atomic attachment of nanocrystals in 2D honeycomb superlattices. *Science* 2014, 344, 1377–1380.
- [16] Baumgardner, W. J.; Whitham, K.; Hanrath, T. Confined-but-connected quantum solids via controlled ligand displacement. *Nano Lett.* 2013, 13, 3225–3231.
- [17] Whitham, K.; Yang, J.; Savitzky, B. H.; Kourkoutis, L. F.; Wise, F.; Hanrath, T. Charge transport and localization in atomically coherent quantum dot solids. *Nat. Mater.* 2016, 15, 557–563.
- [18] Walravens, W.; De Roo, J.; Drijvers, E.; Brinck, S. T.; Solano, E.; Dendooven, J.; Detavernier, C.; Infante, I.; Hens, Z. Chemically triggered formation of two-dimensional epitaxial quantum dot superlattices. ACS Nano 2016, 10, 6861–6870.
- [19] Abelson, A.; Qian, C.; Salk, T.; Luan, Z. Y.; Fu, K.; Zheng, J. G.; Wardini, J. L.; Law, M. Collective topo-epitaxy in the self-assembly of a 3D quantum dot superlattice. *Nat. Mater.* **2020**, *19*, 49–55.
- [20] Balazs, D. M.; Matysiak, B. M.; Momand, J.; Shulga, A. G.; Ibáñez, M.; Kovalenko, M. V.; Kooi, B. J.; Loi, M. A. Electron mobility of 24 cm²·V⁻¹·s⁻¹ in PbSe colloidal-quantum-dot superlattices. *Adv. Mater.* 2018, 30, 1802265.
- [21] Walravens, W.; Solano, E.; Geenen, F.; Dendooven, J.; Gorobtsov, O.; Tadjine, A.; Mahmoud, N.; Ding, P. P.; Ruff, J. P. C.; Singer, A. et al. Setting carriers free: Healing faulty interfaces promotes delocalization and transport in nanocrystal solids. ACS Nano 2019, 13, 12774–12786.
- [22] Jazi, M. A.; Janssen, V. A. E. C.; Evers, W. H.; Tadjine, A.; Delerue, C.; Siebbeles, L. D. A.; Van Der Zant, H. S. J.; Houtepen, A. J.; Vanmaekelbergh, D. Transport properties of a two-dimensional PbSe

- square superstructure in an electrolyte-gated transistor. *Nano Lett.* **2017**, *17*, 5238–5243.
- [23] Evers, W. H.; Schins, J. M.; Aerts, M.; Kulkarni, A.; Capiod, P.; Berthe, M.; Grandidier, B.; Delerue, C.; Van Der Zant, H. S. J.; Van Overbeek, C. et al. High charge mobility in two-dimensional percolative networks of PbSe quantum dots connected by atomic bonds. *Nat. Commun.* 2015, 6, 8195.
- [24] Kalesaki, E.; Delerue, C.; Smith, C. M.; Beugeling, W.; Allan, G.; Vanmaekelbergh, D. Dirac cones, topological edge states, and nontrivial flat bands in two-dimensional semiconductors with a honeycomb nanogeometry. *Phys. Rev. X* 2014, 4, 011010.
- [25] Kalesaki, E.; Evers, W. H.; Allan, G.; Vanmaekelbergh, D.; Delerue, C. Electronic structure of atomically coherent square semiconductor superlattices with dimensionality below two. *Phys. Rev. B* 2013, 88, 115431.
- [26] Dasilva, J. C.; Smeaton, M. A.; Dunbar, T. A.; Xu, Y. Z.; Balazs, D. M.; Kourkoutis, L. F.; Hanrath, T. Mechanistic insights into superlattice transformation at a single nanocrystal level using nanobeam electron diffraction. *Nano Lett.* 2020, 20, 5267–5274.
- [27] Chen, I. Y.; Dasilva, J. C.; Balazs, D. M.; Smeaton, M. A.; Kourkoutis, L. F.; Hanrath, T.; Clancy, P. The role of dimer formation in the nucleation of superlattice transformations and its impact on disorder. ACS Nano 2020, 14, 11431–11441.
- [28] Balazs, D. M.; Dunbar, T. A.; Smilgies, D. M.; Hanrath, T. Coupled dynamics of colloidal nanoparticle spreading and self-assembly at a fluid-fluid interface. *Langmuir* 2020, 36, 6106–6115.
- [29] Minemawari, H.; Yamada, T.; Matsui, H.; Tsutsumi, J.; Haas, S.; Chiba, R.; Kumai, R.; Hasegawa, T. Inkjet printing of single-crystal films. *Nature* 2011, 475, 364–367.
- [30] Nallan, H. C.; Sadie, J. A.; Kitsomboonloha, R.; Volkman, S. K.; Subramanian, V. Systematic design of jettable nanoparticle-based inkjet inks: Rheology, acoustics, and jettability. *Langmuir* 2014, 30, 13470–13477.
- [31] Derby, B. Inkjet printing of functional and structural materials: Fluid property requirements, feature stability, and resolution. *Ann. Rev. Mater. Res.* 2010, 40, 395–414.
- [32] Derby, B. Inkjet printing ceramics: From drops to solid. J. Eur. Ceram. Soc. 2011, 31, 2543–2550.
- [33] Alamán, J.; Alicante, R.; Peña, J. I.; Sánchez-Somolinos, C. Inkjet printing of functional materials for optical and photonic applications. *Materials* 2016, 9, 910.
- [34] Nayak, L.; Mohanty, S.; Nayak, S. K.; Ramadoss, A. A review on inkjet printing of nanoparticle inks for flexible electronics. *J. Mater. Chem. C* 2019, 7, 8771–8795.
- [35] Böberl, M.; Kovalenko, M. V.; Gamerith, S.; List, E. J. W.; Heiss, W. Inkjet-printed nanocrystal photodetectors operating up to 3 μm wavelengths. Adv. Mater. 2007, 19, 3574–3578.
- [36] YousefiAmin, A.; Killilea, N. A.; Sytnyk, M.; Maisch, P.; Tam, K. C.; Egelhaaf, H. J.; Langner, S.; Stubhan, T.; Brabec, C. J.; Rejek, T. et al. Fully printed infrared photodetectors from PbS nanocrystals with perovskite ligands. ACS Nano 2019, 13, 2389–2397.
- [37] Sliz, R.; Lejay, M.; Fan, J. Z.; Choi, M. J.; Kinge, S.; Hoogland, S.; Fabritius, T.; De Arquer, F. P. G.; Sargent, E. H. Stable colloidal quantum dot inks enable inkjet-printed high-sensitivity infrared photodetectors. ACS Nano 2019, 13, 11988–11995.
- [38] Noda, Y.; Minemawari, H.; Matsui, H.; Yamada, T.; Arai, S.; Kajiya, T.; Doi, M.; Hasegawa, T. Underlying mechanism of inkjet printing of uniform organic semiconductor films through antisolvent crystallization. Adv. Funct. Mater. 2015, 25, 4022–4031.
- [39] Al-Milaji, K. N.; Secondo, R. R.; Ng, T. N.; Kinsey, N.; Zhao, H. Interfacial self-assembly of colloidal nanoparticles in dual-droplet inkjet printing. Adv. Mater. Interfaces 2018, 5, 1701561.
- [40] Bealing, C. R.; Baumgardner, W. J.; Choi, J. J.; Hanrath, T.; Hennig, R. G. Predicting nanocrystal shape through consideration of surfaceligand interactions. ACS Nano 2012, 6, 2118–2127.
- [41] Hassinen, A.; Moreels, I.; De Nolf, K.; Smet, P. F.; Martins, J. C.; Hens, Z. Short-chain alcohols strip X-type ligands and quench the luminescence of PbSe and CdSe quantum dots, acetonitrile does not. *J. Am. Chem. Soc.* 2012, *134*, 20705–20712.
- [42] Kirmani, A. R.; Carey, G. H.; Abdelsamie, M.; Yan, B. Y.; Cha, D.; Rollny, L. R.; Cui, X. Y.; Sargent, E. H.; Amassian, A. Effect of

environment on colloidal-quantum-dot solar-cell manufacturability and performance. Adv. Mater. 2014, 26, 4717-4723.

- [43] Balazs, D. M.; Dirin, D. N.; Fang, H. H.; Protesescu, L.; Brink, G. H. T.; Kooi, B. J.; Kovalenko, M. V.; Loi, M. A. Counterion-mediated ligand exchange for PbS colloidal quantum dot superlattices. ACS Nano 2015, 9, 11951-11959.
- [44] Jang, D.; Kim, D.; Moon, J. Influence of fluid physical properties on ink-jet printability. Langmuir 2009, 25, 2629-2635.
- [45] Tai, J. Y.; Gan, H. Y.; Liang, Y. N.; Lok, B. K. Control of droplet formation in inkjet printing using Ohnesorge number category: Materials and processes. In 2008 10th Electronics Packaging Technology Conference, Singapore, 2008, pp 761–766.
- [46] Russel, W. B.; Saville, D. A.; Schowalter, W. R. Colloidal Dispersions; Cambridge University Press: Cambridge, 1991.
- [47] Doblas, D.; Kister, T.; Cano-Bonilla, M.; González-García, L.; Kraus, T. Colloidal solubility and agglomeration of apolar nanoparticles in different solvents. Nano Lett. 2019, 19, 5246-5252.
- [48] Krieger, I. M.; Dougherty, T. J. A mechanism for Non-Newtonian flow in suspensions of rigid spheres. Trans. Soc. Rheol. 1959, 3,
- [49] Aveyard, R.: Haydon, D. A. Thermodynamic properties of aliphatic hydrocarbon/water interfaces. Trans. Faraday Soc. 1965, 61, 2255-2261.
- [50] Zeppieri, S.; Rodríguez, J.; De Ramos, A. L. L. Interfacial tension of alkane + water systems. J. Chem. Eng. Data 2001, 46, 1086-1088.

- [51] Geuchies, J. J.; Van Overbeek, C.; Evers, W. H.; Goris, B.; De Backer, A.; Gantapara, A. P.; Rabouw, F. T.; Hilhorst, J.; Peters, J. L.; Konovalov, O. et al. In situ study of the formation mechanism of two-dimensional superlattices from PbSe nanocrystals. Nat. Mater. 2016, 15, 1248-1254.
- [52] Weidman, M. C.; Smilgies, D. M.; Tisdale, W. A. Kinetics of the self-assembly of nanocrystal superlattices measured by real-time in situ X-ray scattering. Nat. Mater. 2016, 15, 775-781.
- [53] Whitham, K.; Smilgies, D. M.; Hanrath, T. Entropic, enthalpic, and kinetic aspects of interfacial nanocrystal superlattice assembly and attachment. Chem. Mater. 2018, 30, 54-63.
- [54] Whitham, K.; Hanrath, T. Formation of epitaxially connected quantum dot solids: Nucleation and coherent phase transition. J. Phys. Chem. Lett. 2017, 8, 2623-2628.
- [55] Peters, J. L.; Van Der Bok, J. C.; Hofmann, J. P.; Vanmaekelbergh, D. Hybrid oleate-iodide ligand shell for air-stable PbSe nanocrystals and superstructures. Chem. Mater. 2019, 31, 5808-5815.
- [56] Peng, X. X.; Abelson, A.; Wang, Y.; Qian, C.; Shangguan, J. Y.; Zhang, Q. B.; Yu, L.; Yin, Z. W.; Zheng, W. J.; Bustillo, K. C. et al. In situ TEM study of the degradation of PbSe nanocrystals in air. Chem. Mater. 2019, 31, 190-199.
- [57] Gao, Y. J.; Huang, J. Y.; Balazs, D. M.; Xu, Y. Z.; Hanrath, T. Photoinitiated transformation of nanocrystal superlattice polymorphs assembled at a fluid interface. Adv. Mater. Interfaces 2020, 7, 2001064.